

Test beam proton calorimetry note

Josh Devan

June 20, 2014

Abstract

This is the abstract.

This is the text.

1 Results

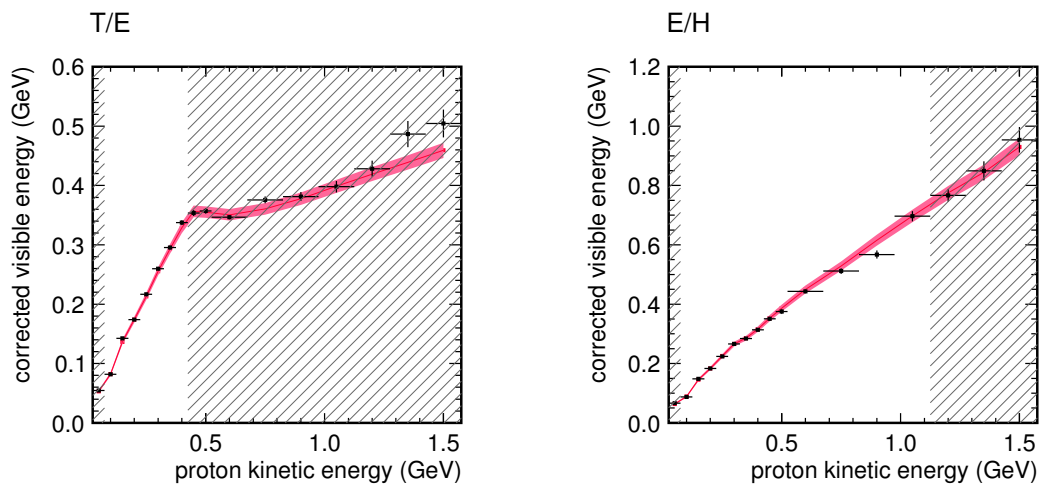


Figure 1: Mean of calorimetric energy vs. proton kinetic energy. Data in black with statistical errors. MC in red with systematic errors.

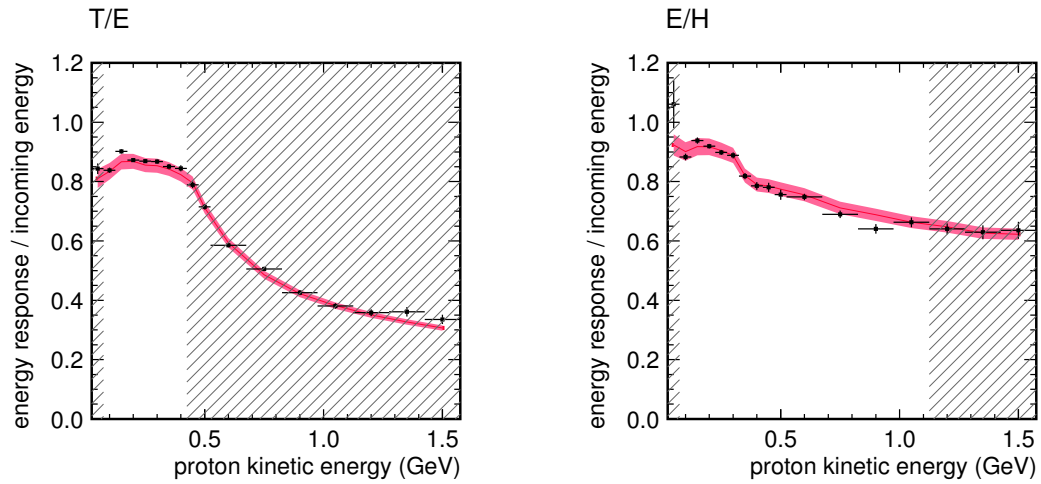


Figure 2: Mean of calorimetric energy / KE vs. proton kinetic energy. Data in black with statistical errors. MC in red with systematic errors.

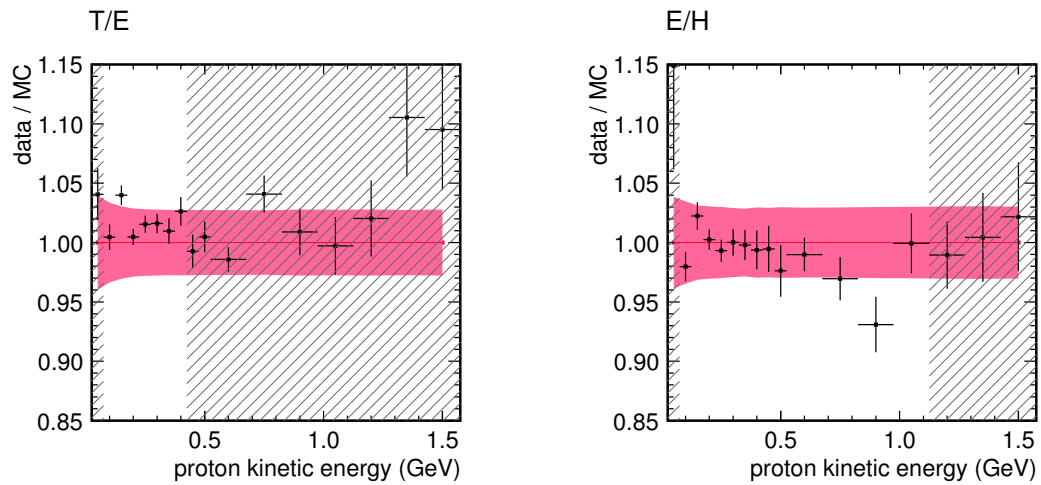


Figure 3: Data/MC ratio of Figure 2 (mean of calorimetric energy / KE vs. proton kinetic energy). Data in black with statistical errors. MC in red with systematic errors.

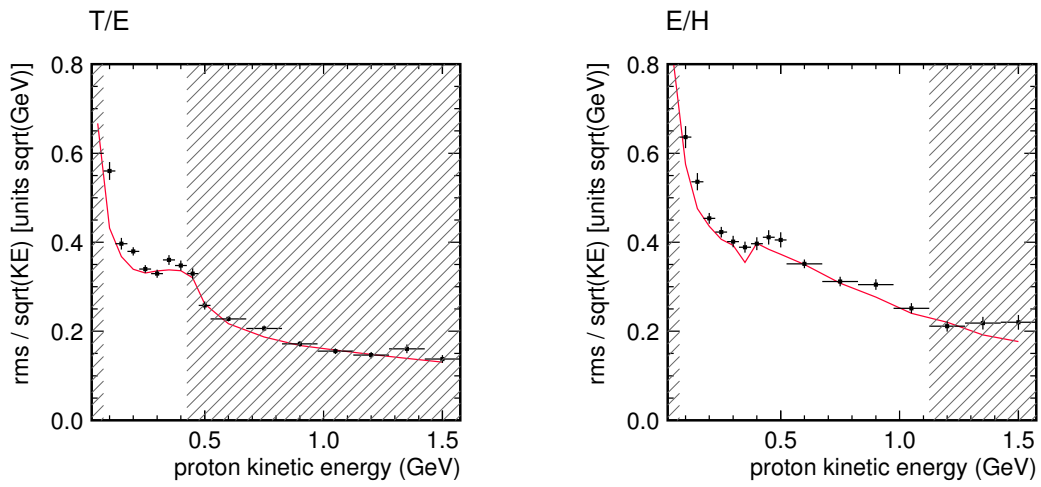


Figure 4: RMS of calorimetric energy / KE vs. proton kinetic energy. Data in black with statistical errors. MC in red with systematic errors.

2 Systematic errors

2.1 Calibration and energy scale

The test beam detector calibration is described in tech note TN018, docdb:8686.

2.1.1 MEU/LY

The energy scale calibration procedure produces two constants: MEU (muon equivalent unit) and LY (light yield). LY converts from photons to photoelectrons (PE) in the MC, by matching the photoelectrons observed in the data. MEU converts from PE to MeV, by matching the MC truth energy deposited in the active scintillator of the detector planes. The calibration is performed with through-going muons depositing MIP-scale energies.

TN018 gives the uncertainty on the energy scale arising from the MEU/LY tuning as 1.1% on the absolute scale and 0.6% on data/MC comparisons. The dominant components of the uncertainty are the intrinsic uncertainty of the polynomial fit to the energy distributions and an unexplained difference in the MEU factor between the T/E and E/H detectors.

2.1.2 Cross-talk

A measurement of the cross-talk in data finds an average of $4.2 \pm 0.5\%$ over the first 25 planes. The cross-talk in MC is scaled to this value. The MEU calibration, however, only considers energy deposited on the muon track and thus is tuning $100 - 4.2\% = 95.8\%$ of the PE to 100% of the true deposited MeV. This results in the absolute energy scale being high by 4.2%. For this and other calorimetry analyses, the absolute response of data and MC is scaled down by this value.

2.1.3 LPos effect

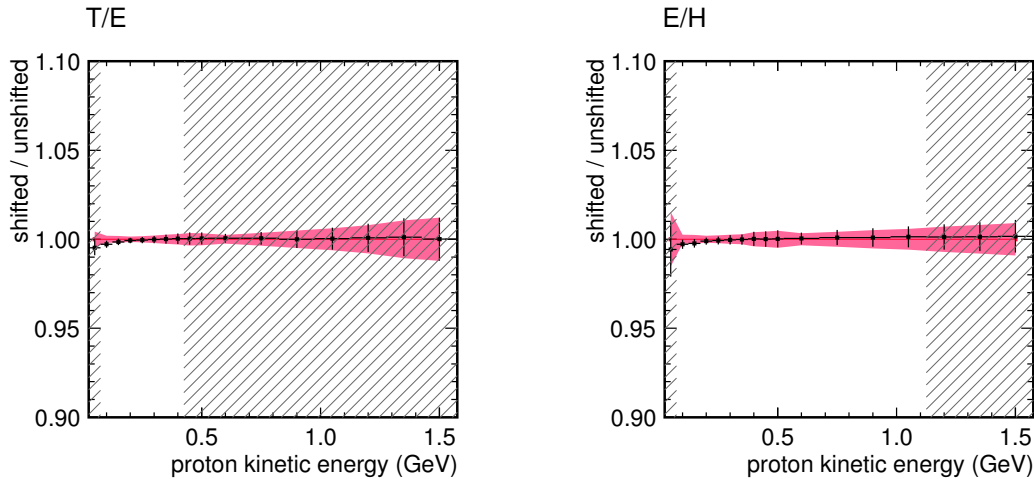


Figure 5: LPos effect; a residual position-dependent calibration error observed only in the data.¹

The LPos (longitudinal position) effect is a position-dependent calibration discrepancy between the data and MC. In the data, it is observed that (after attenuation correction), the calibrated energy varies across the length of a strip. The final cause was never determined; an incorrect measurement or application of attenuation is a possibility (TN018 describes the problem in greater detail). The

kludge tool, WilliamClayFordSystematicsTool, provides a means of generating a shifted MC sample including the LPos effect observed in data. Figure 5 shows the ratio of shifted to unshifted energy response / incoming energy versus proton KE. The effect is 0.3% at 100 MeV, becoming even more negligible at high energy. It is included in the error band as energy-dependent.

2.1.4 PMT non-linearity

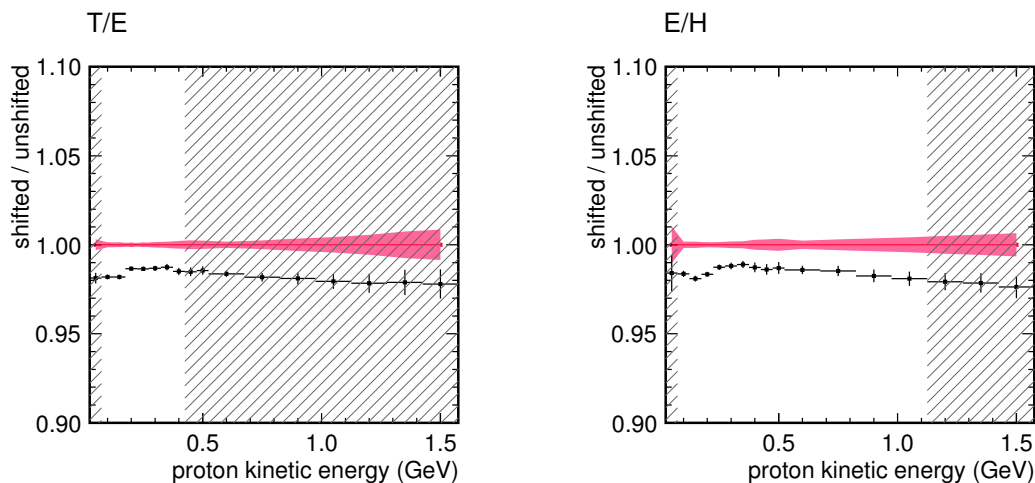


Figure 6: PMT non-linearity (2σ).¹

PMT non-linearity is not currently modeled in the MC, but TBAna includes code to compute a 2σ correction based on a calculation by Howard Budd (details in TN018). Figure 6 shows the ratio of shifted (with non-linearity) to unshifted (without non-linearity, the default) MC. The 1σ effect is 0.7% constant across energy. While this is actually a one-sided uncertainty (non-linearity can only decrease the energy response), it is incorporated symmetrically.

PMT non-linearity is evaluated here for a single proton, but could potentially be a more significant uncertainty in the big detector for multi-particle final states and large EM showers. The effect should be included in the systematic error on the calorimetric reconstruction of the recoil system.

2.1.5 Birks' constant

Birks' constant and uncertainty are determined by Rik's stopping proton analysis (see TN037, docdb:9131). Figures 7 and 8 show the ratio of shifted to unshifted MC for $\pm 15\%$ (1σ) variations. The effect is 2.3% at 100 MeV and 1.2% (T/E) 1.5% (E/H) at higher KE. A change to Birks' constant affects the MEU tuning, should the full calibrations be re-performed. For a 15% shift in Birks' constant, the MEU shifts by 0.3%. This component of the uncertainty is already included with the MEU and is subtracted from the energy-dependent Birks' uncertainty, yielding a final uncertainty of 2.0% at 100 MeV and 0.9% (T/E) 1.2% (E/H) at higher KE.

¹Statistical errors (\sqrt{n}) for the unshifted MC are plotted in red; for the shifted MC are plotted in black on the ratio. But these are identical Geant-simulated events (the shift is applied during calibration), so the error is effectively zero.

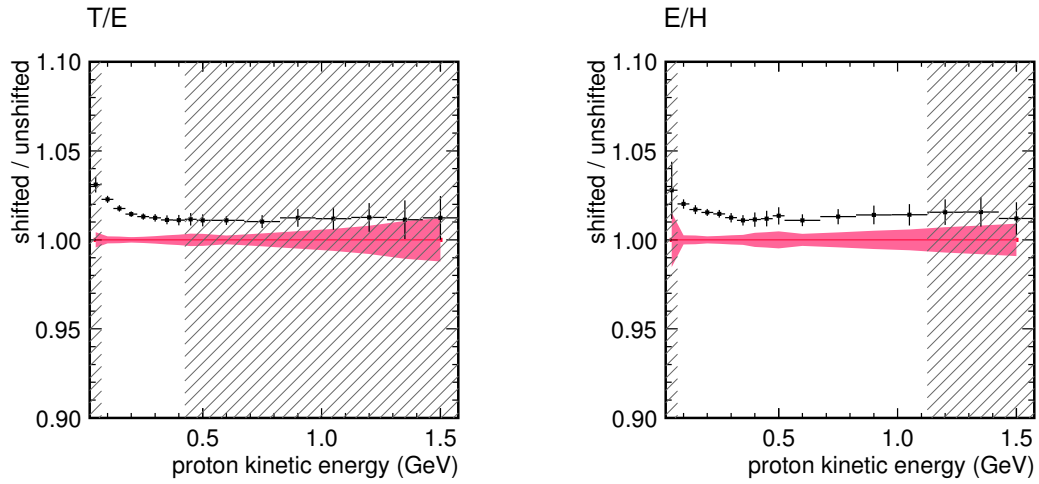


Figure 7: Birks' constant -15% .¹

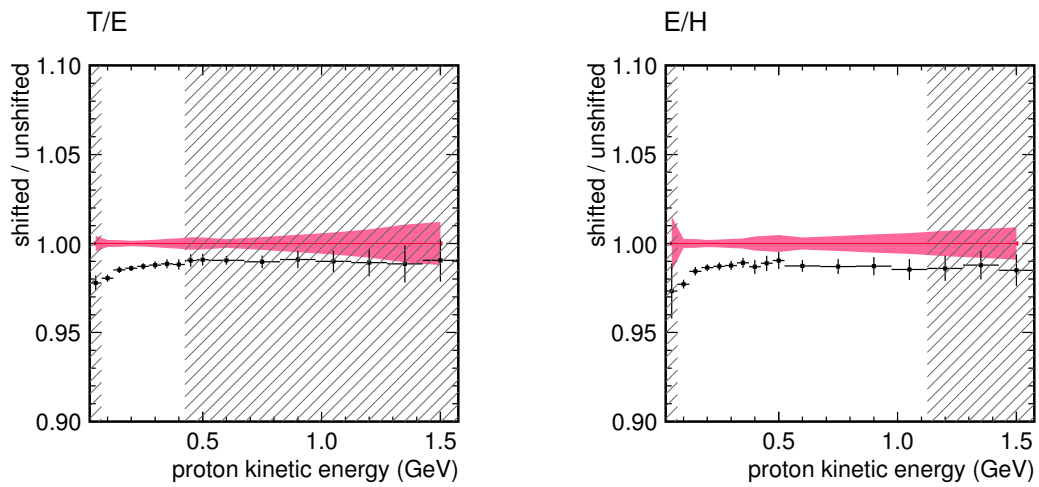


Figure 8: Birks' constant $+15\%$.¹

2.2 Mass model

The uncertainty on the scintillator plane mass model has two components: the total amount of material and the active fraction. The uncertainty on the total material in a scintillator plane is 1.5%. The uncertainty on the active fraction is much larger at 3–5% and has not been well evaluated. For a calorimetry analysis, however, the active fraction cancels out and we can take the smaller 1.5% uncertainty.

The argument (interpreted from TN018) is that through the LY tuning, the PE in the MC is matched to that in the data. The MEU is then set to convert from this PE to the MC truth energy deposited in the active part of the scintillator plane, which is effectively the active fraction times the total deposition in the plane. For calorimetry, we correct to the total deposition in the plane by dividing by the active fraction. There is a small effect from different photostatistics, but the dominant uncertainty is on the energy deposited in an entire plane by a through going muon, which is given by the total material uncertainty.

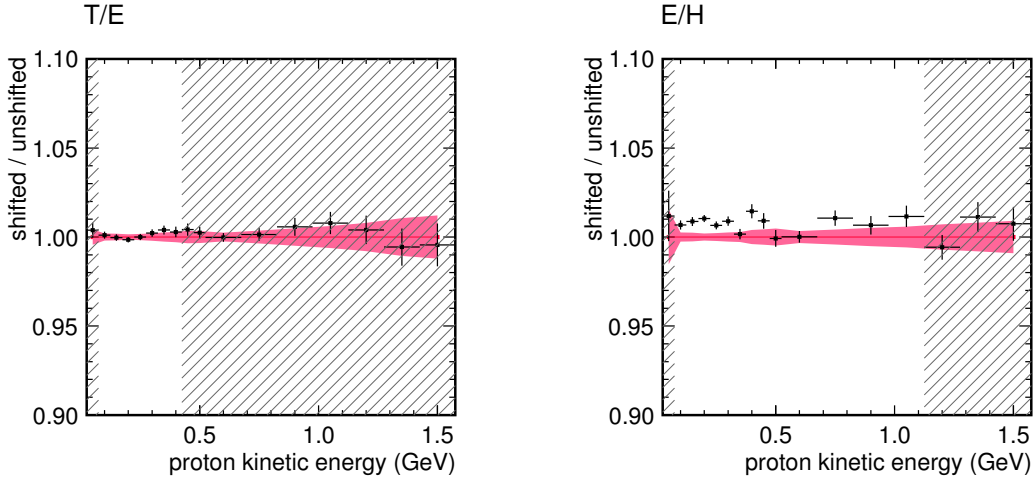


Figure 9: Pb density -2.4% (2σ).

Figures 9, 10 and 11 show the ratio of shifted to unshifted MC for 2σ variations in the lead and iron of the ECAL and HCAL sub-detectors. The 1σ uncertainty from the lead mass is taken as 0.2% for the T/E detector in the 300 MeV bin and above and 0.4% constant for the E/H detector. The 1σ uncertainty from the iron mass is taken as 0.4% for the E/H detector in the 400 MeV bin and above.

Figure 12 shows the ratio of shifted to unshifted MC for a 2σ variation in the thickness of the aluminum foils in the wire chambers of the tertiary beamline. The 1σ effect is 0.7% at 100 MeV. It is implemented as an energy-dependent systematic with a value of 0.7% at 100 MeV, linearly falling to zero at 300 MeV.

2.3 Beamline momentum

The beamline resolution and systematic errors are documented in TN017, docdb:8547.

The uncertainty on the beamline momentum has four components: a momentum-dependent alignment uncertainty of 1.0% per GeV/c (i.e. 0.5% at 500 MeV/c, 1.0% at 1 GeV/c) and three constant magnetic field uncertainties of 0.5%. The four are added in quadrature to form the final momentum uncertainty. Figures 13 and 14 show the ratio of shifted to unshifted MC for a positive and negative shift in beamline momentum. The uncertainty is taken as 1.9% constant.

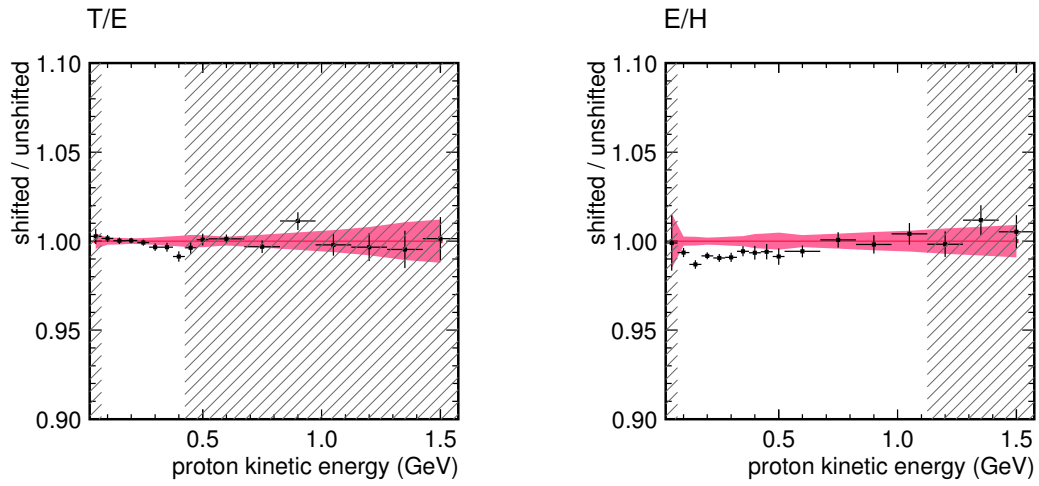


Figure 10: Pb density +2.4% (2σ).

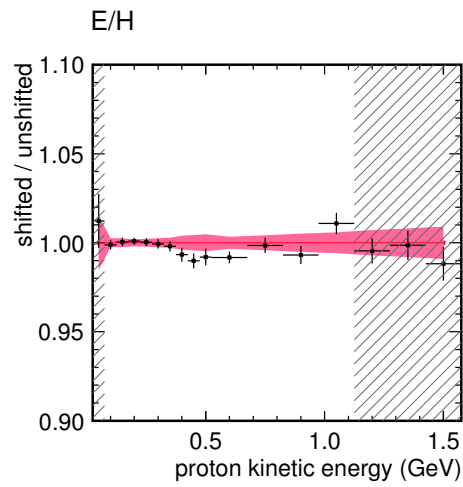


Figure 11: Fe density +2.0% (2σ).

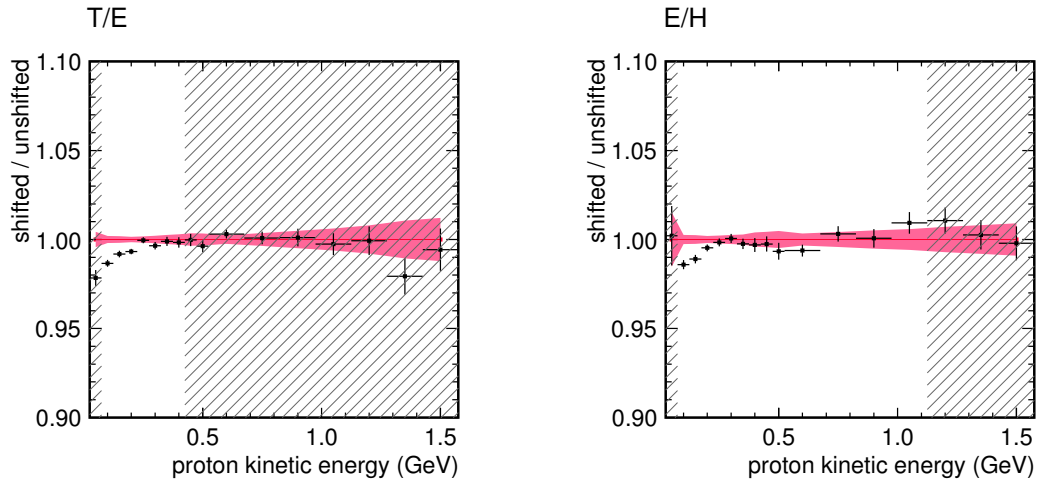


Figure 12: Thickness of wire chamber aluminum foils +400% (2σ).

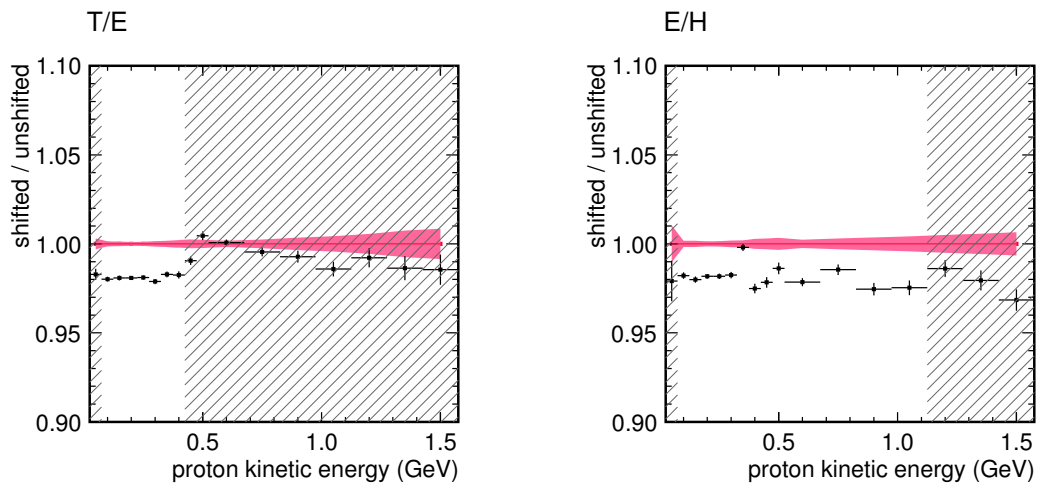


Figure 13: Beamline momentum shifted up.

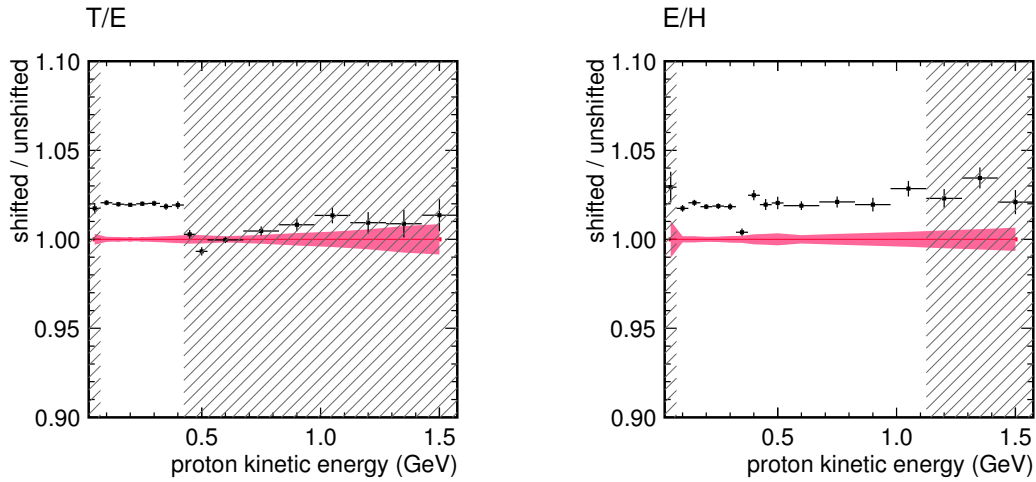


Figure 14: Beamline momentum shifted down.

2.4 Stability

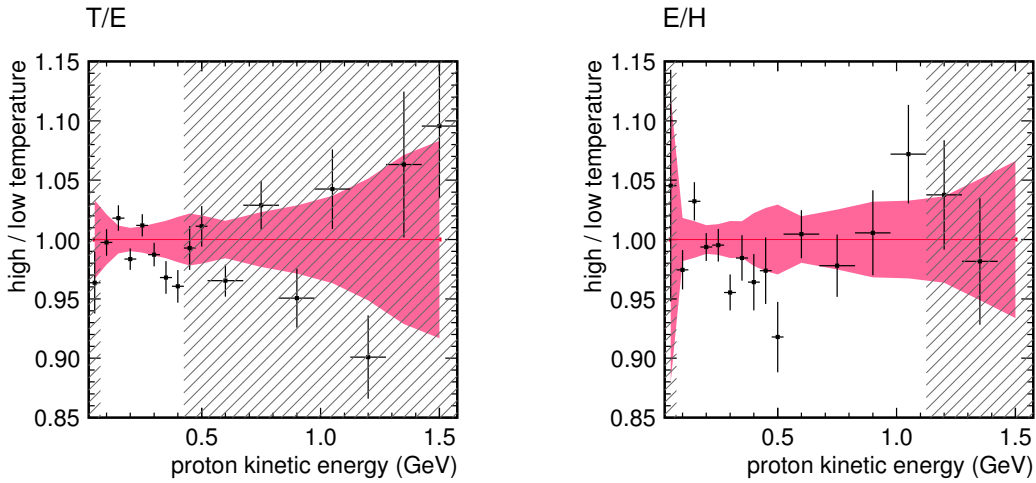


Figure 15: Temperature stability.

The temperature in the experiment hall varied wildly during the Summer 2010 run due to a failed HVAC unit. The temperature was lowest at 4 AM for the start of data taking and highest at 6 PM when beam was disabled. The average hall temperature rose as the run proceeded later into Summer. A correction was implemented as described in TN018. The correction uses the temperature probe located near the test beam detector and connected to ACNET to correct the approximately -0.4% per degree Celsius degradation in energy response with rising temperature.

Figure 15 shows the stability of the data after this correction through the ratio of high temperature data ($> 28\text{ C}$) to low temperature data ($< 28\text{ C}$). No distinguishable trend is observed, so no additional systematic uncertainty is included.

Figure 16 divides the data set by vertical position at the most downstream wire chamber (WC4).

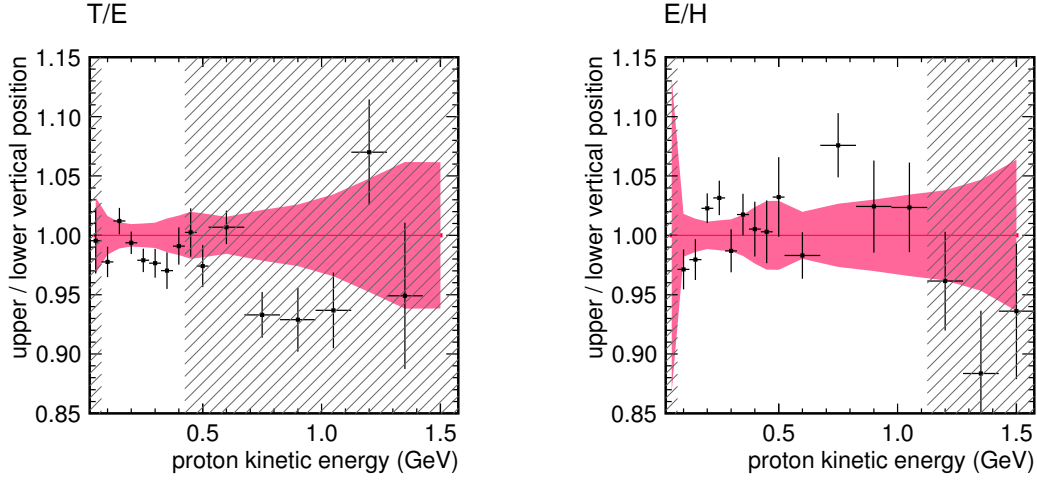


Figure 16: Vertical position stability.

Again, no trend is observed. The equivalent plot for horizontal position is not utilized because horizontal position is correlated with particle momentum.

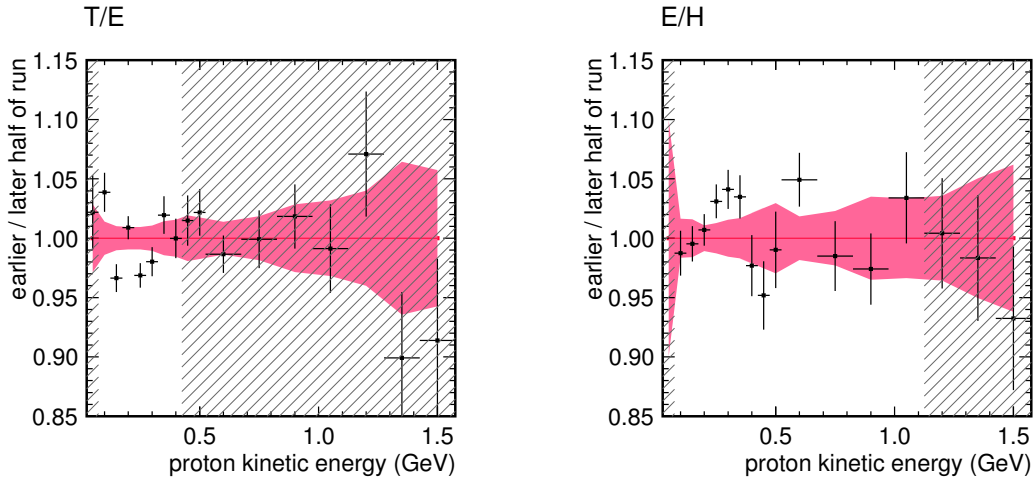


Figure 17: Time stability.

Figure 17 divides the data set by time, plotting the ratio of the first and second half of the T/E and E/H runs. No trend is observed.

2.5 Event selection

The default beamline selection is the “loose” beamline cuts; as a systematic study, we implement the “strict” cuts, which includes additional limits on the magnetic field integral, the magnetic error integral (the magnetic error is non-zero in the more questionable regions of the field) and the fit χ^2 . Figure 18 is a double ratio of data/MC energy response / incoming energy of the strict cuts over

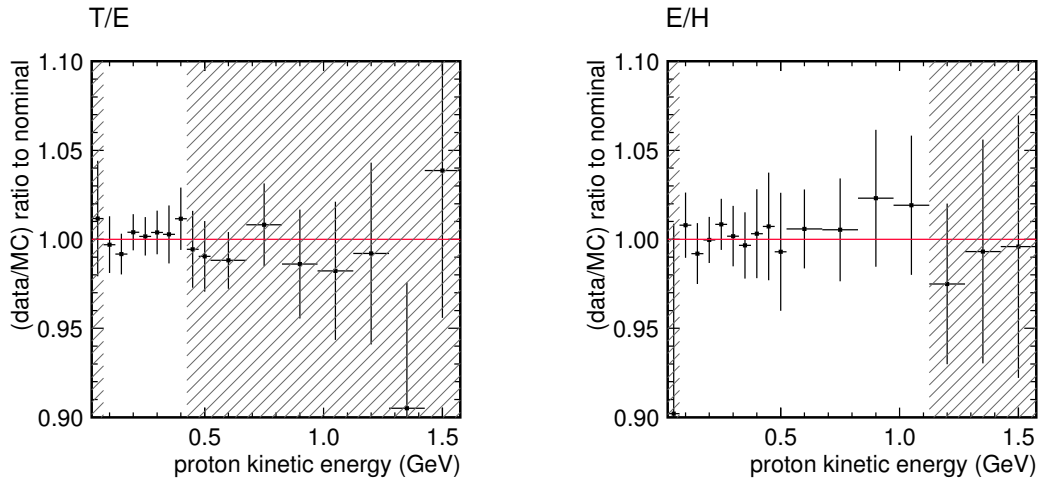


Figure 18: Strict beamline quality cuts.

the default cuts. The strict cuts are not expected to affect the MC in any way other than varying the momentum distribution of protons. As evidenced in the plot, the data is not affected either.

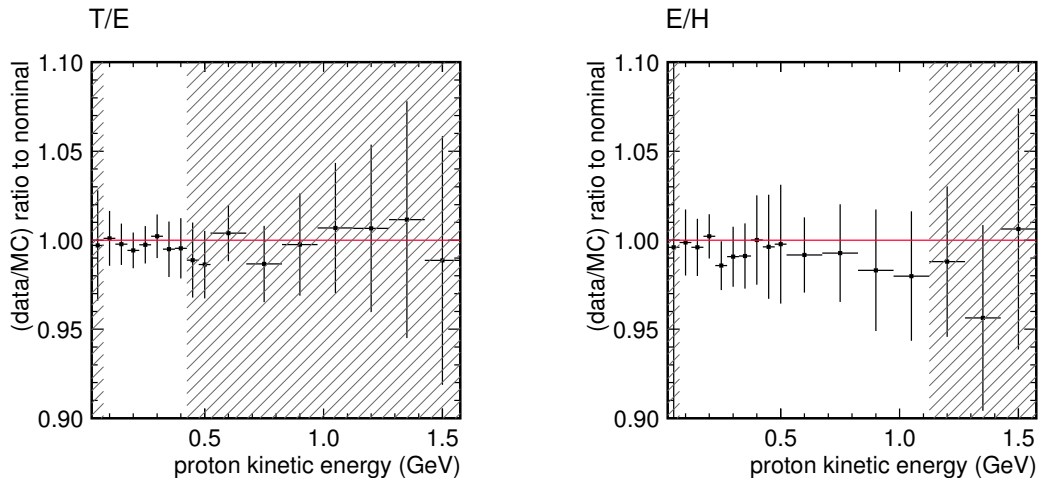


Figure 19: Cut events with an adjacent time slice within $(-800, 400)$ ns ($2 \times$ default window).

The default beamline selection cuts events with an adjacent time slice less than 400 ns before or 200 ns after the primary slice. This removes events with dead time from earlier activity and events that are part of large cascades from an upstream shower that generate many time slices. The time window is doubled to 800 ns before or 400 ns after as a systematic study, shown in Figure 19. The effect is 0.3% in the T/E detector and 0.6% in the E/H detector, taken as a constant.

The origin of this systematic is not immediately clear; adjacent time slices can be caused by beam backgrounds (only in the data), PMT after-pulsing, late neutron hits, Michel electrons and other decay products.

2.6 Pile-up background

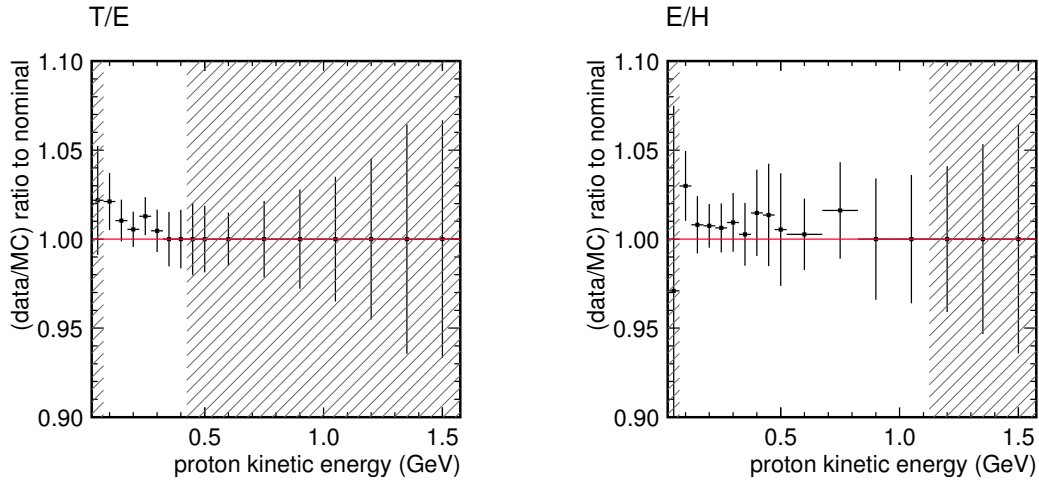


Figure 20: Disable ignoring the downstream sub-detector for low energy events and the pile-up background veto.

The default analysis ignores the downstream sub-detector for the very low energy events to avoid integrating the background of neutrons drifting through the hall from upstream interactions. The downstream sub-detector is utilized as a veto for these events to remove muon and pion contamination. For mid-energy events, the last four planes are used a muon/pion veto. Figure 20 shows the result of disabling these features of the analysis. This is not taken as a systematic, only an illustration of magnitude.

2.7 Calorimetry

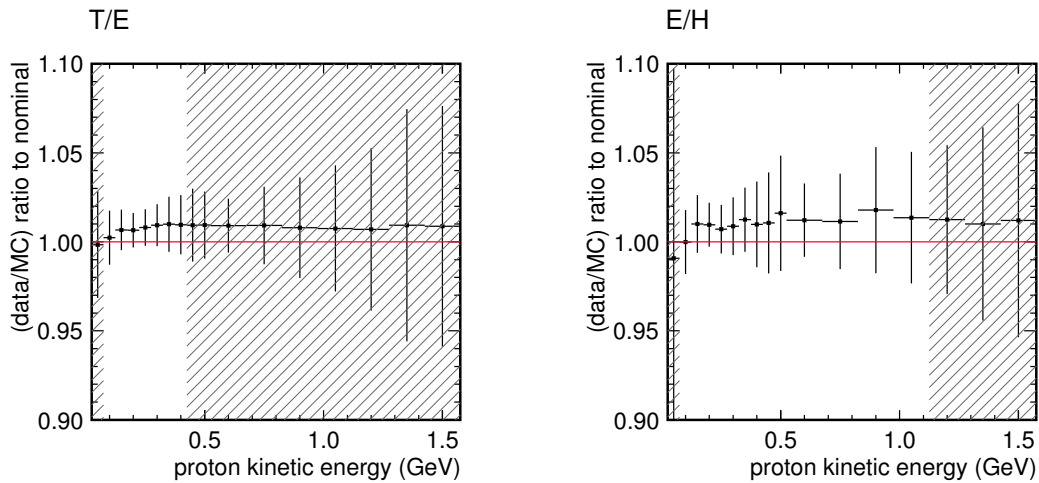


Figure 21: Ignore clusters < 0.5 MeV for calorimetry.

Figure 21 shows the results of ignoring clusters with energy less than 0.5 MeV in the calorimetric sum. The effect is 0.7% in the T/E detector and 0.9% in the E/H detector, constant in energy. A component of the sub 0.5 MeV clusters is clearly cross-talk. TN018 specifies a cross-talk systematic of 0.5%, but for this analysis, the systematic is expanded to 0.7% and 0.9% to cover all low energy response.

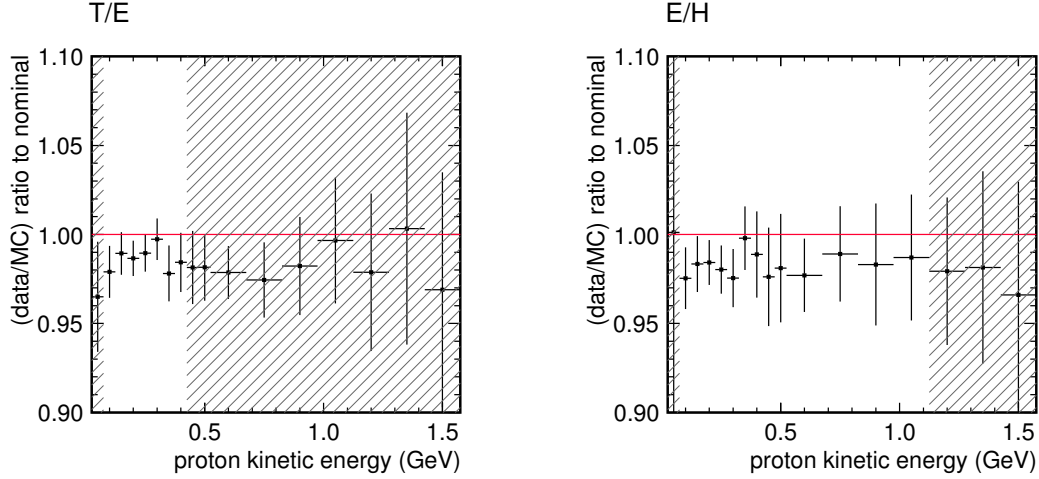


Figure 22: Big detector calorimetry time window (include only clusters within $(-20, 35)$ ns).

For the reconstruction of the recoil system in the CC inclusive analysis in the big detector, only clusters within a $(-20, 35)$ ns window around the vertex time are included. Figure 22 imposes that same cut on the proton calorimetry analysis. The effect is 1.2% (T/E) and 1.7% (E/H). This is not included in the systematic error for this analysis, but the magnitude indicates it should be considered as part of the systematic error for the recoil system in the big detector.

2.8 Summary

The systematic errors on the data/MC ratio of energy response / incoming energy are summarized in Table 1.

error	T/E	E/H
MEU/LY	0.6%	0.6%
cross-talk	0.7%	0.9%
LPos	0.3% (100 MeV)	0.3% (100 MeV)
PMT non-linearity	0.7%	0.7%
Birks' constant	2.0% (100 MeV) 0.9% (400 MeV)	2.0% (100 MeV) 1.2% (1 GeV)
scintillator mass	1.5%	1.5%
lead mass	0.2% (≥ 300 MeV)	0.4%
iron mass	N/A	0.4% (≥ 400 MeV)
WC Al foil mass	0.7% (100 MeV)	0.7% (100 MeV)
beamline momentum	1.9%	1.9%
adjacent time slices	0.3%	0.6%
quadrature sum	3.4% (100 MeV) 2.8% (400 MeV)	3.5% (100 MeV) 3.0% (1 GeV)

Table 1: Summary of systematic errors.

3 Eroica vs. Resurrection

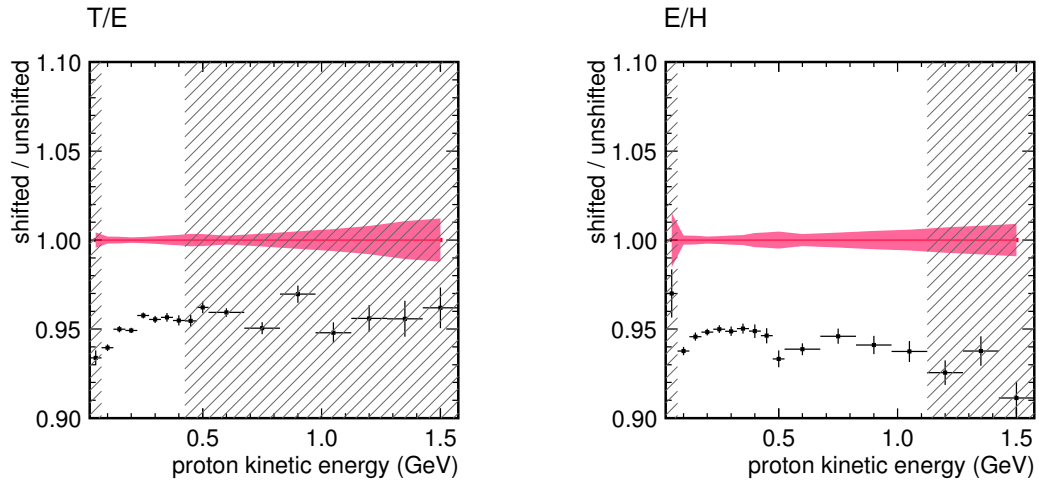


Figure 23: Resurrection-era geometry, hit aggregation, neutron settings and Birks' constant.

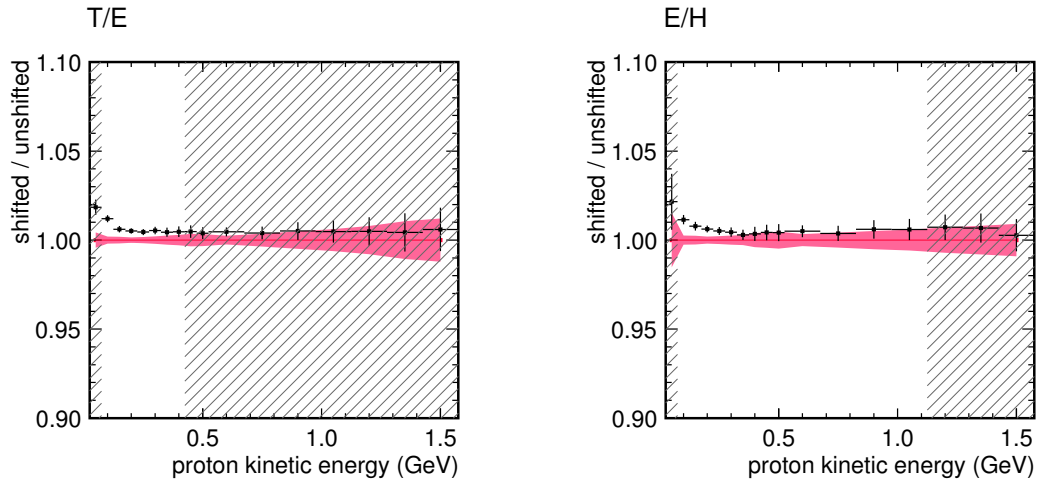


Figure 24: Resurrection-era hit aggregation.

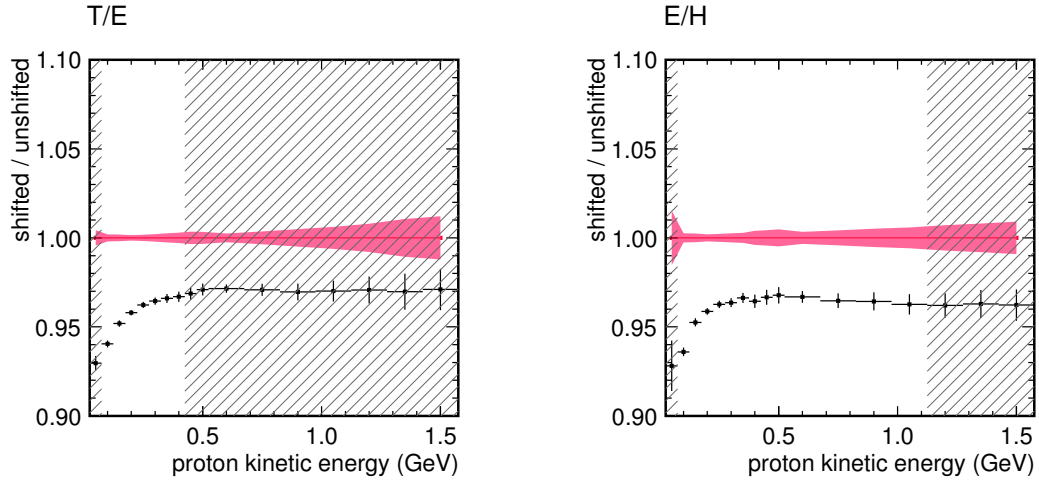


Figure 25: Resurrection-era Birks' constant.

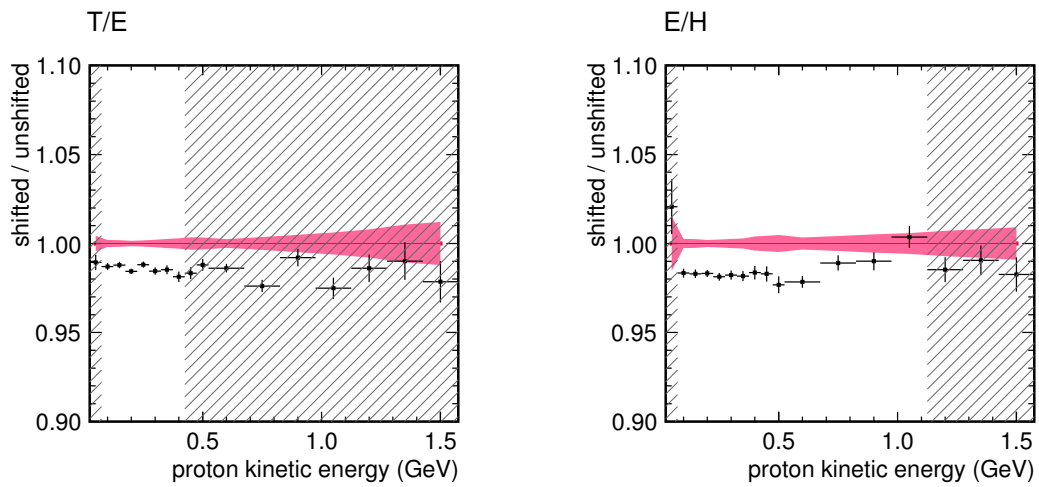


Figure 26: Resurrection-era geometry.

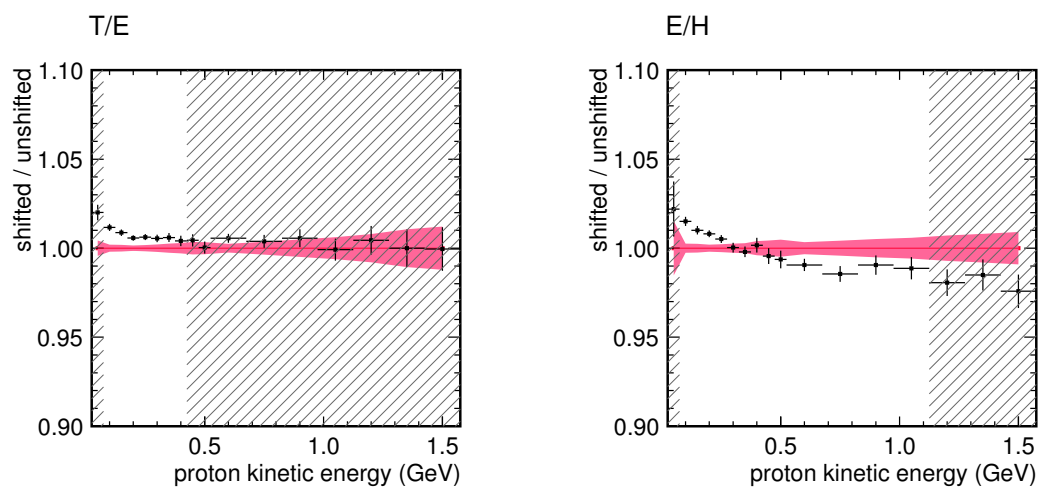


Figure 27: Resurrection-era hit aggregation and neutron settings.